Structure
Article

Inhibition of Caspase-2 by a Designed Ankyrin Repeat Protein: Specificity, Structure, and Inhibition Mechanism

Andreas Schweizer,[1,2,4] Heidi Roschitzki-Voser,[1,4] Patrick Amstutz,[1,3] Christophe Briand,[1] Maya Gulotti-Georgieva,[1] Eva Prenosil,[1] H. Kaspar Binz,[1,3] Guido Capitani,[1] Antonio Baici,[1] Andreas Plückthun,[1] and Markus G. Grütter[1,*]

[1] Department of Biochemistry, University of Zürich, Winterthurerstrasse 190, CH-8057 Zürich, Switzerland
[2] Division of Infectious Diseases and Hospital Epidemiology, Department of Medicine, University Hospital Zürich, Rämistrasse 100, 8091 Zürich, Switzerland
[3] Molecular Partners AG, Grabenstrasse 11a, 8952 Schlieren, Switzerland
[4] These authors contributed equally to this work.
*Correspondence: gruetter@bioc.unizh.ch
DOI 10.1016/j.str.2007.03.014

SUMMARY

Specific and potent caspase inhibitors are indispensable for the dissection of the intricate pathways leading to apoptosis. We selected a designed ankyrin repeat protein (DARPin) from a combinatorial library that inhibits caspase-2 in vitro with a subnanomolar inhibition constant and, in contrast to the peptidic caspase inhibitors, with very high specificity for this particular caspase. The crystal structure of this inhibitor (AR_F8) in complex with caspase-2 reveals the molecular basis for the specificity and, together with kinetic analyses, the allosteric mechanism of inhibition. The structure also shows a conformation of the active site that can be exploited for the design of inhibitory compounds. AR_F8 is a specific inhibitor of an initiator caspase and has the potential to help identify the function of caspase-2 in the complex biological apoptotic signaling network.

INTRODUCTION

Apoptosis, or programmed cell death, is essential for normal development and tissue homeostasis of all multicellular organisms. While excessive apoptosis can cause disorders such as neurodegenerative diseases, insufficient apoptosis is a hallmark of cancer. Caspases (cysteine-dependent aspartyl-specific proteases) are highly specific cysteine proteases, initiating and executing apoptotic cell death (Fuentes-Prior and Salvesen, 2004 and references therein), and some caspases play an important role in inflammation. Eleven human caspases have been identified with distinct functions in apoptosis and inflammation (Fuentes-Prior and Salvesen, 2004; Siegel, 2006). While some caspases are functionally well characterized, others are still poorly understood. Caspase-2 is a classic example of the latter group, as its function has remained enigmatic, mainly because there is no dramatic phenotype of the caspase-2 null mouse (Bergeron et al., 1998). However, a pivotal role of caspase-2 in the initiation of the intrinsic apoptotic pathway has been described (Hanahan and Weinberg, 2000). Caspase-2 appears to act upstream of mitochondrial permeabilization and plays a critical role as the most apical initiator caspase in DNA-damage-induced apoptosis (Guo et al., 2002; Lassus et al., 2002; Robertson et al., 2002, 2004). Moreover, caspase-2 is activated in response to various anticancer agents (Ceruti et al., 2003; Dirsch et al., 2004; Robertson et al., 2002) and was reported to play an important role in breast cancer (Sevignani et al., 2003), in β-amyloid cytotoxicity (Troy et al., 2000), and in leukemia (Estrov et al., 1998; Faderl et al., 1999). A more recent report demonstrates that caspase-2 is activated in a complex containing the death-domain-containing protein PIDD, whose expression is induced by the tumor suppressor p53, indicating that increased PIDD may result in caspase-2 activation in response to genotoxic stress (Tinel and Tschopp, 2004). However, as the intracellular targets of caspase-2, as well as its precise function in apoptosis, remain obscure, further investigations are required for a better understanding of this cell-death protease.

The functional investigation of caspases is challenging, as the close relationship between the different family members makes it difficult to assign a function or a phenotype to a specific caspase. Highly selective inhibitors that function intracellularly would be required to knock out individual caspases at the protein level. Numerous peptidic caspase inhibitors have been developed, but, reflecting the conservation of the active-site region of caspases, the vast majority of them lack sufficient specificity.

A possible strategy that can be used to circumvent this problem relies on the use of proteins as inhibitors to achieve higher selectivity. Currently, the intracellular use of protein-based inhibitors requires transfection of the encoding gene, which limits the use of such inhibitors to discovery tools at this time; however, many strategies for cellular protein uptake and gene therapy (Green

et al., 2003) are under development for future broader use of such inhibitory proteins. This protein-based approach is also complementary to the use of RNAi, as the specificity of such inhibitory RNA is not always perfect, nor is the inhibitory effect always very strong (Jackson et al., 2003; Sledz et al., 2003).

Such proteinaceous inhibitors are not limited to binding the conserved active-site cleft, but could interact with the target enzyme across a different surface, thus increasing the chances for high specificity. Antibodies, which are the most frequently used binding molecules, and also the most common proteins investigated for enzyme inhibition, may not represent the optimal solution to this problem, as their stability depends on disulfide bridges, which cannot form in the reducing environment of the cytoplasm (Biocca et al., 1995; Ewert et al., 2004). With designed ankyrin repeat proteins (DARPins), we have developed an alternative to antibodies. DARPins can be selected to bind any given target protein with high affinity and high specificity (Binz et al., 2004). They are well expressed, highly stable, and do not contain cysteines, making them ideally suited for applications in reducing environments (Amstutz et al., 2005). We report here the selection, isolation, and characterization of DARPin AR_F8, which is the first, to our knowledge, specific caspase-2 inhibitor. In addition, the crystal structure of the caspase-2/AR_F8 complex is presented, which reveals the molecular interactions and, together with kinetic analyses, the mechanism of inhibition that explains the unprecedented selectivity for caspase-2.

RESULTS

Ribosome Display

Ribosome-display selection rounds with an N3C DARPin library, consisting of an N-terminal capping repeat, three randomized repeats, and a C-terminal capping repeat, were performed on immobilized caspase-2 as described (Hanes and Plückthun, 1997). The theoretical diversity of the N3C library is 3.8×10^{23}, and the DNA library used in the selection contained at least 10^{10} individual members, as estimated from the amount of ligated library DNA (Binz et al., 2004). The diversity of the library was further increased by introducing random errors through the polymerase in subsequent PCR cycles. An enrichment of binders was already observed after the second ribosome-display selection round, but three selection rounds were performed before analyzing the selected library members. This yielded a pool of caspase-2-binding DARPins that served as the starting point for a combined solid-phase screen for binders and inhibitors.

Combined Solid-Phase Assay to Screen for Binding and Inhibition

The pool of selected DARPins was screened for caspase-2 inhibitors and binders by a combined solid-phase screen (Figure 1A). The high expression level of DARPins allowed for expression and subsequent analysis of selected DARPins in a 96-well format. Caspase-2 was immobilized via a biotinylation tag on neutravidin. The crude bacterial extracts, each containing one specific DARPin, were added to immobilized caspase-2, and, after extensive washing, caspase-2 activity was analyzed (Figure 1A, upper panel). After washing, binding of DARPins was detected by an enzyme-linked immunosorbent assay (ELISA) (Figure 1A, lower panel). Approximately 60 DARPins showed specific binding to caspase-2 in the ELISA screen (signal/background $\geq$ 2), whereas unselected DARPins showed no interaction with immobilized caspase-2 (data not shown). Among the 60 specific caspase-2 binders identified, one, named AR_F8, significantly inhibited caspase-2 in the solid-phase caspase activity assay. AR_F8 was subsequently purified to homogeneity for further investigations.

Stoichiometry of the Caspase-2/AR_F8 Complex

The stoichiometry of the caspase-2/AR_F8 complex in solution was investigated by multiangle light scattering. The molecular mass was determined to be 97,000 ± 400 Da, suggesting that two AR_F8 molecules bind to the caspase-2 dimer, a finding that is consistent with the results obtained by X-ray crystallography (see below).

Analysis of Binding and Inhibition

The affinity of the caspase-2/AR_F8 interaction was investigated by kinetic surface plasmon resonance (SPR) measurements (see Figure S1 and the Supplemental Data available with this article online). Association and dissociation experiments at various concentrations of AR_F8 with immobilized caspase-2 yielded a dissociation constant of K_D = 4.1 nM, indicating high-affinity binding.

The diagnosis of the kinetic mechanism of AR_F8-mediated inhibition of caspase-2 was performed with the specific velocity plot (Figure S2), Equation 1 (Experimental Procedures), followed by refinement with Equation 2 (Experimental Procedures) for tight-binding, hyperbolic inhibition applied to the data shown in Figure 1B. The overall kinetic mechanism can be classified as tight-binding, hyperbolic mixed-type, with a more competitive than uncompetitive character. Referring to Scheme 1 (Experimental Procedures), the kinetic parameters at 25°C and pH = 6.50 were: $\alpha = 2.9 \pm 0.8$, $\beta = 0.04 \pm 0.01$, $K_i = 0.29 \pm 0.02$ nM, where α is the ratio of the competitive to the uncompetitive inhibitor constant, and β is the fraction of the turnover rate of the inhibited enzyme relative to the uninhibited one. Thus, the inhibitor constant of the competitive branch in Scheme 1 was 0.29 nM, and that of the uncompetitive component was 0.29 nM multiplied by α, i.e., 0.84 nM. When performing nonlinear regression with Equation 2, it was necessary to fit the active enzyme concentration, because the procedure requires an exact knowledge of the active-site concentration; however, only approximate values can be determined experimentally, since no suitable caspase-2 active-site titrant is available to date. The best-fit value of the total enzyme concentration was 2.3 ± 0.1 nM (active site), while the concentration estimated from protein content was 1 nM (dimer concentration). This analysis agrees with structural

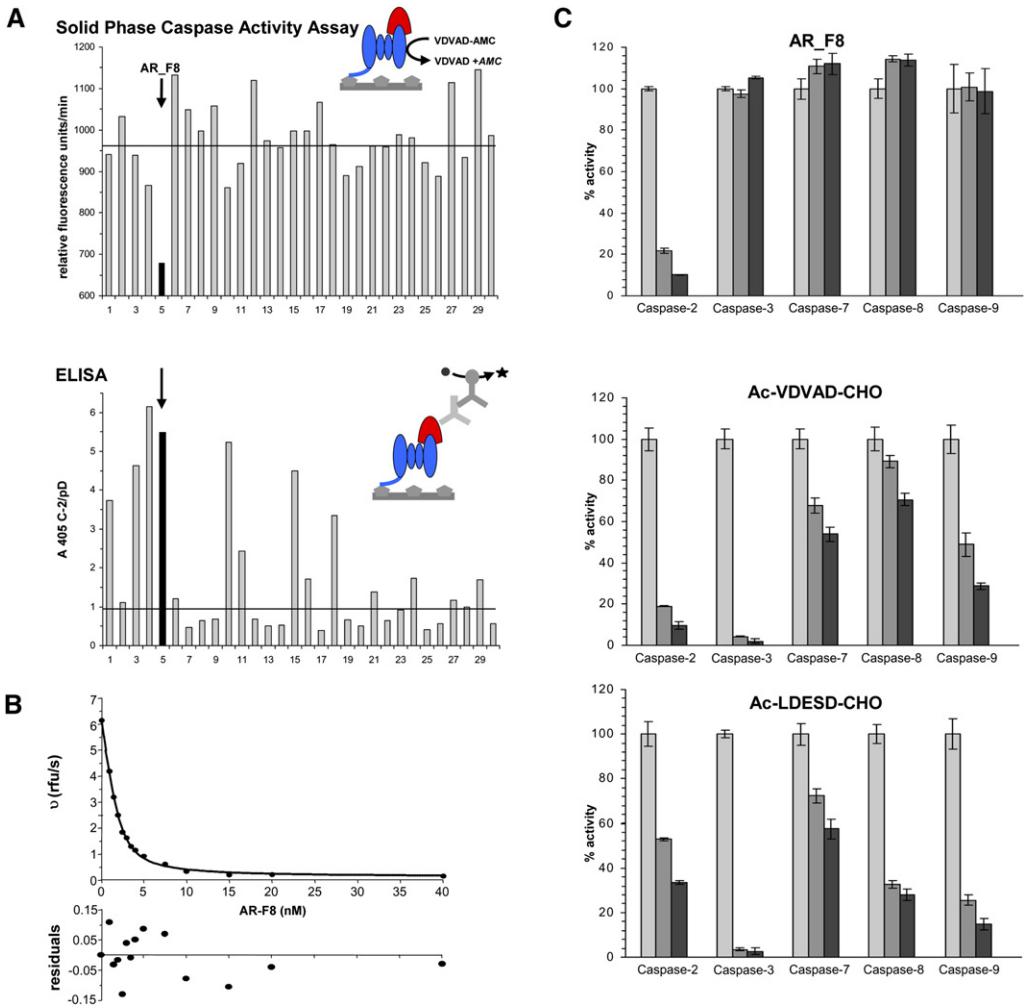

Figure 1. Combined Solid-Phase Screen for Binders and Inhibitors

(A) The upper panel represents the caspase activity assay. The assay is carried out with the fluorescent substrate Ac-VDVAD-AMC (20 μM) in complex with caspase-2 (20 nM), immobilized via a biotinylation tag on neutravidin, in the presence of 30 different candidate DARPins. The dashed line indicates the mean enzymatic activity of the 30 assays. As shown in the lower panel, an ELISA was then used for detection of binding. The ratios of the binding signal of the candidate protein on caspase-2 and on control wells, which were coated with protein D from phage λ, are given. Values above 1 (dashed line) indicate better binding on caspase-2 than on the control surface. The signal obtained for AR_F8 is indicated with an arrow. The schematic setup of each assay is also depicted; caspase-2 is shown in blue, the DARPin is shown in red, and the primary and secondary antibodies are shown in light and dark gray, respectively. p-nitrophenylphosphate (black) was used as the substrate for the ELISA. The two assays were performed sequentially in the same 96-well plate. The DARPins were assayed in the form of crude *E. coli* extracts from 1.2 ml 96-well cultures.

(B) Inhibition of caspase-2 (1 nM) by AR_F8 (1–40 nM). The solid line shows the nonlinear least-squares fit on the enzyme activity (relative fluorescence units per second) for tight-binding conditions (Szedlacsek et al., 1988); residuals are given below.

(C) AR_F8 inhibits caspase-2 specifically. The specificity of the DARPin was examined by measuring AR_F8-mediated inhibition of caspase-2, -3, -7, -8, and -9. The results are compared with inhibition data of the two commercially available caspase-2 inhibitors, Ac-VDVAD-CHO and Ac-LDESD-CHO. The first column (light gray) stands for the enzymatic activity of the uninhibited caspase (= 100%), the second column (dark gray) stands for 60 nM inhibitor, and the third column (black) stands for 150 nM inhibitor. All caspases, with the exception of caspase-9, which was assayed at 150 nM, were adjusted to a concentration of 30 nM, while caspase-9 was assayed at 150 nM; for caspase-9 inhibition was tested at 300 nM and 750 nM. The substrate Ac-VDVAD-AMC was used at 20 μM. Error bars refer to standard deviation of three individual measurements.

data, revealing two independent active sites on the enzyme.

The apparent discrepancy between the dissociation constant obtained by SPR analysis (K_D = 4.1 nM) and the inhibitor constants determined kinetically (K_i = 0.29 nM, αK_i = 0.84 nM) can be sought in the different experimental approaches. A biotinylated, Avi-tagged variant of the caspase was used to immobilize the enzyme for SPR measurements. It is likely that in this system AR_F8 has binding properties slightly different from those kinetically measured in solution in the presence of a substrate. Moreover, the uncompetitive branch of the inhibition mechanism, involving the formation of a ternary ESI complex, cannot be seen in the SPR experiment.

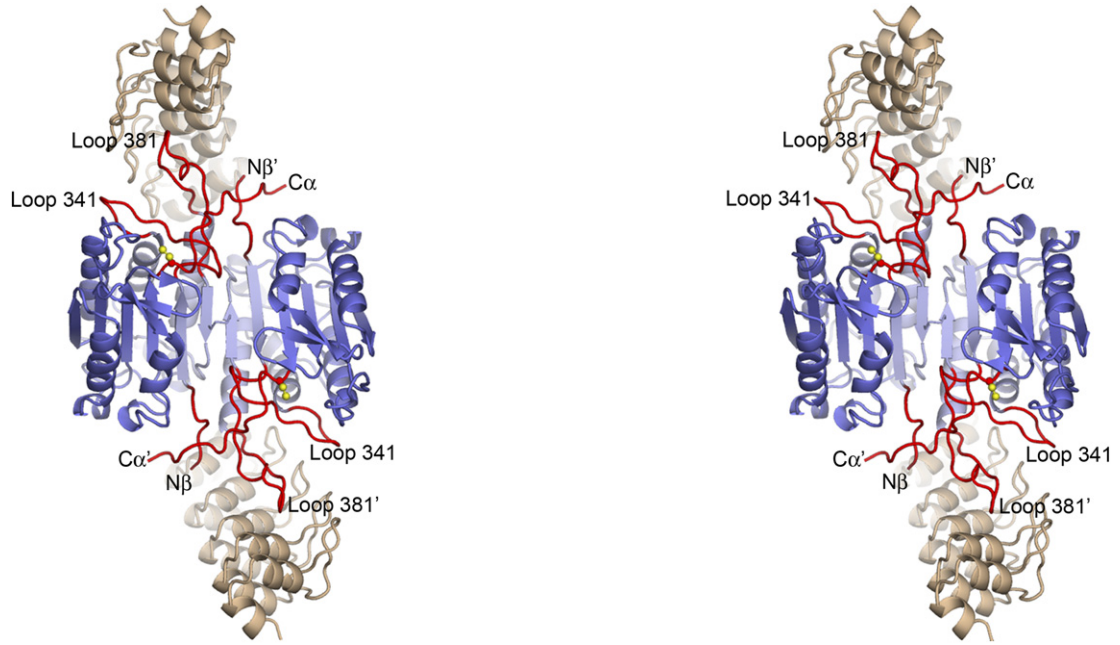

Figure 2. Stereo Representation of the Structure of the Caspase-2/AR_F8 Complex

Caspase-2 is shown in dark blue (α subunit) and light blue (β subunit), and AR_F8 is shown in salmon. AR_F8 is bound to the back side of the active-site-forming loop 381 (see Figure 5C) of each caspase-2 monomer. Termini and loops affected by binding of AR_F8 are shown in red. The active-site cysteine (Cys285) and the intersubunit disulfide bond are shown in yellow.

In summary, tight-binding, mixed-type inhibition of the hyperbolic type with a subnanomolar K_i value was determined for caspase-2 inhibition by AR_F8. Mixed-type inhibition with a significant uncompetitive contribution indicates that AR_F8 binds the enzyme-substrate complex and the free enzyme with comparable affinity, and that AR_F8 does not substantially compete for binding to the active site of caspase-2. Hence, the kinetic data are consistent with our structural model, in which the AR_F8 inhibitor does not bind in the active site, but interacts elsewhere with the dimeric caspase-2 and thus functions as an allosteric effector.

Specificity of AR_F8

To investigate the specificity of AR_F8, inhibition of caspase-2 by AR_F8 was compared to the effect of AR_F8 on caspases-3, -7, -8, and -9, which represent the closest homologs of caspase-2 in terms of sequence identity and substrate specificity. AR_F8 was compared with commercially available caspase-2 inhibitors, the penta-peptide aldehydes Ac-VDVAD-CHO and Ac-LDESD-CHO. Our results demonstrate that AR_F8 exclusively inhibits caspase-2, but none of the other caspases tested (Figure 1C). Caspase-1, a representative of the cytokine activators, was not inhibited by AR_F8 either (data not shown). The peptidic aldehyde caspase-2 inhibitors, in contrast, suppressed the enzymatic activity of all tested members of the caspase family, albeit to varying extents (Figure 1C). Consistent with literature data (Talanian et al., 1997), Ac-VDVAD-CHO, commonly employed as a caspase-2-specific compound, inhibits caspase-3 better than caspase-2, and all other caspases tested show clearly reduced enzymatic activities in the presence of this compound. Ac-LDESD-CHO, used as a caspase-2 and -3 inhibitor, revealed an even more pronounced preference for caspase-3, but it also inhibits all other representatives of the caspase family. To test whether AR_F8 leads to unspecific inhibition when applied at higher concentrations, the experiment was repeated for caspases-3, -7, and -8 at concentrations of AR_F8 of 300 nM (10-fold molar excess), 600 nM (20-fold excess), and 1.2 μM (40-fold excess), respectively. Even at these high concentrations no trace of inhibition was detected, underscoring the specificity of the selected inhibitor (data not shown). Due to the low enzymatic activity, caspase-9 had to be assayed separately (150–600 nM) and was not inhibited by the addition of greater amounts of AR_F8 (tested up to 3 μM; data not shown).

Structure of the Caspase-2/AR_F8 Complex

The caspase-2/AR_F8 complex crystallized in space group $P2_1$, with three complexes with a molecular mass of 98,081 Da in the asymmetric unit. The three independent complexes show similar conformations, and, in each complex, two AR_F8 molecules bind to a caspase-2 dimer (Figure 2). The coordinates of the molecule with chains A, B, C, D, P, and Q were used in all figures. The concave surface of AR_F8, harboring most of the randomized amino acids, binds to loop 381 of the caspase-2 β subunit (the numbering refers to the insertion point in

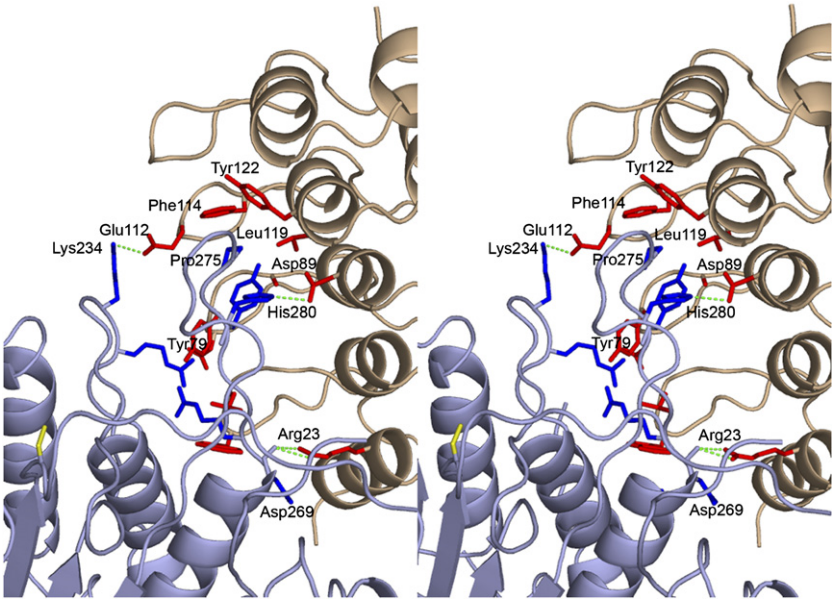

Figure 3. Molecular Interactions between AR_F8 and Caspase-2

Stereo representation of the caspase-2/AR_F8 interface rotated ~90° from the standard orientation, viewed from the back plane of the caspase, displaying hydrogen bonds (green, dotted lines) and hydrophobic interactions. Interacting residues of AR_F8 are shown in red; those of caspase-2 are shown in blue.

caspase-1, see Figure 5C), which forms one rim of the active-site cleft of the enzyme. Additional interactions are observed with the N-terminal segment of the symmetry-related β subunit of caspase-2 (Figure 2). When superimposing the structures of the caspase-2/AR_F8 complex and of Ac-LDESD-CHO bound to caspase-2 (Schweizer et al., 2003), differences are observed in all segments forming the active site (Figure 2 and discussed below).

The interaction surface of the caspase-2/AR_F8 complex was analyzed by using the protein-protein interaction server (http://www.biochem.ucl.ac.uk/bsm/PP/server) and the Protein Interfaces, Surfaces, and Assemblies (PISA) server (http://www.ebi.ac.uk/msd-srv/prot_int/pistart.html). The buried accessible surface area (ASA) on AR_F8 is, on average, 852 Å^2, with a planarity index of 2.5 and a surface complementarity of 0.60, involving 24 residues of caspase-2 and 25 residues of AR_F8, respectively. The global protein-protein interaction parameters obtained are comparable to other known ankyrin repeat protein-target protein complexes, to antibody-antigen interfaces, and to other heterodimeric protein-protein interfaces (Binz et al., 2004; Amstutz et al., 2005; Lo Conte et al., 1999).

Comparison with the Caspase-2/LDESD-CHO Structure

To describe the interactions in detail, we use the numbering of the enzyme presented in the PDB file; standard numbering of caspase-1 (Fuentes-Prior and Salvesen, 2004) is given in parentheses. Due to a hydrophobic interaction primarily involving Phe114 of AR_F8 and Pro275 (381c) as well as Gly276 (381d) of caspase-2, loop 381 is shifted by 1 Å toward AR_F8, resulting in an opening of the active-site cleft compared to other caspase-2/peptide inhibitor structures (Figures 3, 4, 5A, and 5B). In complex with AR_F8, Met209 (319) of the N-terminal part of the adjacent symmetry-related β subunit of caspase-2 is involved in a hydrophobic contact with Thr57 of AR_F8 and is observed 3 Å away from its position in the caspase-2/LDESD complex (Schweizer et al., 2003). In this conformation, the C-terminal part of the α subunit is shifted, resulting in a displacement of the active-site Cys155 (285) by 1 Å compared to its position when bound to peptidic inhibitors (Figure 4). In addition, the conformation of the β strand at the bottom of the active-site cleft, which is involved in the precise positioning of peptidic inhibitors, and presumably substrates, through a network of hydrogen bonds, is different in the caspase-2/AR_F8 complex, affecting the structural organization of the S1-, S2-, and S3-binding pockets (Figures 4, 5A, and 5B). The global positioning of residues involved in ligand binding is only moderately affected. The disruption of the hydrogen-bonding network and the shift of the active-site cysteine, however, prevent correct binding, and thus cleavage of substrates. Furthermore, the side chain of Tyr79 of AR_F8 interacts with caspase-2 close to its S5 pocket, and the side chain of Glu112 of AR_F8 forms a hydrogen bond with Lys234 (344) of caspase-2, affecting the S4 subpocket. Thus, binding of AR_F8 also stabilizes a different caspase-2 conformation for the S4 and the S5 substrate-binding pockets with altered shape and physical properties (Figure 4). This renders the extended active site inaccessible to substrates (Figures 5A and 5B).

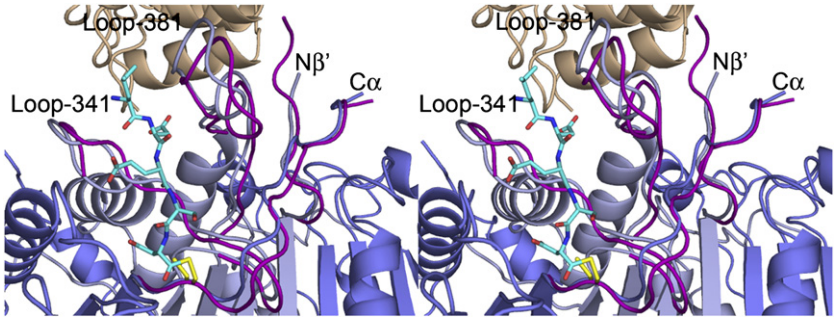

Figure 4. Superposition of the Active Sites of the Caspase-2/Ac-LDESD-CHO and the Caspase-2/AR_F8 Structures

AR_F8 is shown in salmon, caspase-2 is shown in dark blue (large α subunit) and light blue (small β subunit), and the active-site cysteine is shown in yellow. In the bound form, loop 381 is shifted toward the AR_F8 inhibitor. The N-terminal part of the symmetry-related β subunit (Nβ′) is in a different position from that observed in the caspase-2/LDESD-CHO complex (caspase loops, magenta; the peptide aldehyde is colored by atom type), resulting in a rearrangement of the C-terminal part of the α subunit (Cα) with the active-site cysteine. Also, the location of the β strand that forms the bottom of the active site as well as the adjacent loop 341 is altered.

It is a well-known fact that the active-site regions of caspases are flexible and show a high degree of adaptability when interacting with different inhibitors. In contrast to active-site-directed inhibitors, however, AR_F8 inhibits the enzyme by stabilizing an inactive, but probably preexisting, conformation, a finding that is consistent with the structural investigation of other DARPin inhibitor complexes (Kohl et al., 2005; Sennhauser et al., 2007).

DISCUSSION

Most of the numerous substrate-derived caspase inhibitors exhibit very low specificity for a particular caspase. Such inhibitors may be useful if the activity of the entire family, comprised of initiators and effectors of apoptosis as well as cytokine activators, is to be suppressed (Garcia-Calvo et al., 1998; Talanian et al., 1997). However, with the possible exception of Ac-VYAD-CHO, a reasonably specific caspase-1 inhibitor, peptidic caspase inhibitors cannot discriminate sufficiently between individual caspases (Garcia-Calvo et al., 1998). Some nonpeptidic isatin caspase inhibitors have been reported to selectively inhibit caspase-3 and caspase-7, and the anilino-quinazolines inhibit caspase-3 and, to some extent, caspase-6 (Scott et al., 2003); however, despite these advances, highly selective inhibitors of caspases are still very difficult to design.

A fundamental disadvantage of conventional caspase inhibitors is that they all target the conserved active-site region, resulting in poor specificity of these compounds. As protein surfaces display higher variability, specificity can be increased if binding of the inhibitor is instead targeted to the surface of caspases. Protein binders are known to interact with their targets, forming a large interaction area; hence, they appear to be optimal for achieving high selectivity. Antibodies are often used for this purpose, and some enzyme-inhibiting antibodies have also been described. The use of recombinant antibodies as intracellular inhibitors is limited since they contain intradomain disulfide bridges that contribute significantly to stability (Biocca et al., 1995; Ewert et al., 2004). DARPins bind their targets in an antibody-like manner (Binz et al., 2004), but they contain no cysteines. Here, we show that DARPins can act as highly specific, highly potent caspase inhibitors that are functional under reducing conditions, such as those found in the cell.

The high specificity of AR_F8 can be explained by the fact that AR_F8 binds to two flexible surface regions of caspase-2, primarily loop 381 and the N-terminal segment of the β subunit. This selects a conformation with differences in regions directly interacting with AR_F8 (N-terminal peptide of the β subunit, loop 341, loop 381) and in the β strand adjacent to loop 341 that forms the bottom of the active-site cavity. The caspase surfaces involved in binding display highly diverse sequence segments among all human caspases (Figure 5C). These sequence segments, with the exception of Asp269 (379), which is replaced by Glu in the mouse enzyme, are identical in human and murine caspase-2. Therefore, we assume that AR_F8 also interacts with the murine enzyme, albeit with decreased affinity.

These findings are in line with those from a previous study on the selection of a DARPin-based inhibitor of a prokaryotic kinase that was shown to be fully active in vitro and in vivo, indicating the potential of DARPins as intracellular inhibitors (Amstutz et al., 2005). The intrinsic stability of the DARPin consensus structure results in a high percentage of functional library members, minimizing the occurrence of unfolded proteins within the library. This reduces unspecific interactions that might otherwise be caused by "sticky" hydrophobic patches. Since DARPins are well expressed as soluble proteins, we could employ a combined solid-phase screen for binders and inhibitors in a 96-well format, which allows for testing of crude bacterial extracts. This procedure may be easily automated and is by no means limited to caspases; it may be adapted to any other enzyme with an appropriate activity assay. Binding of DARPins is not restricted to the

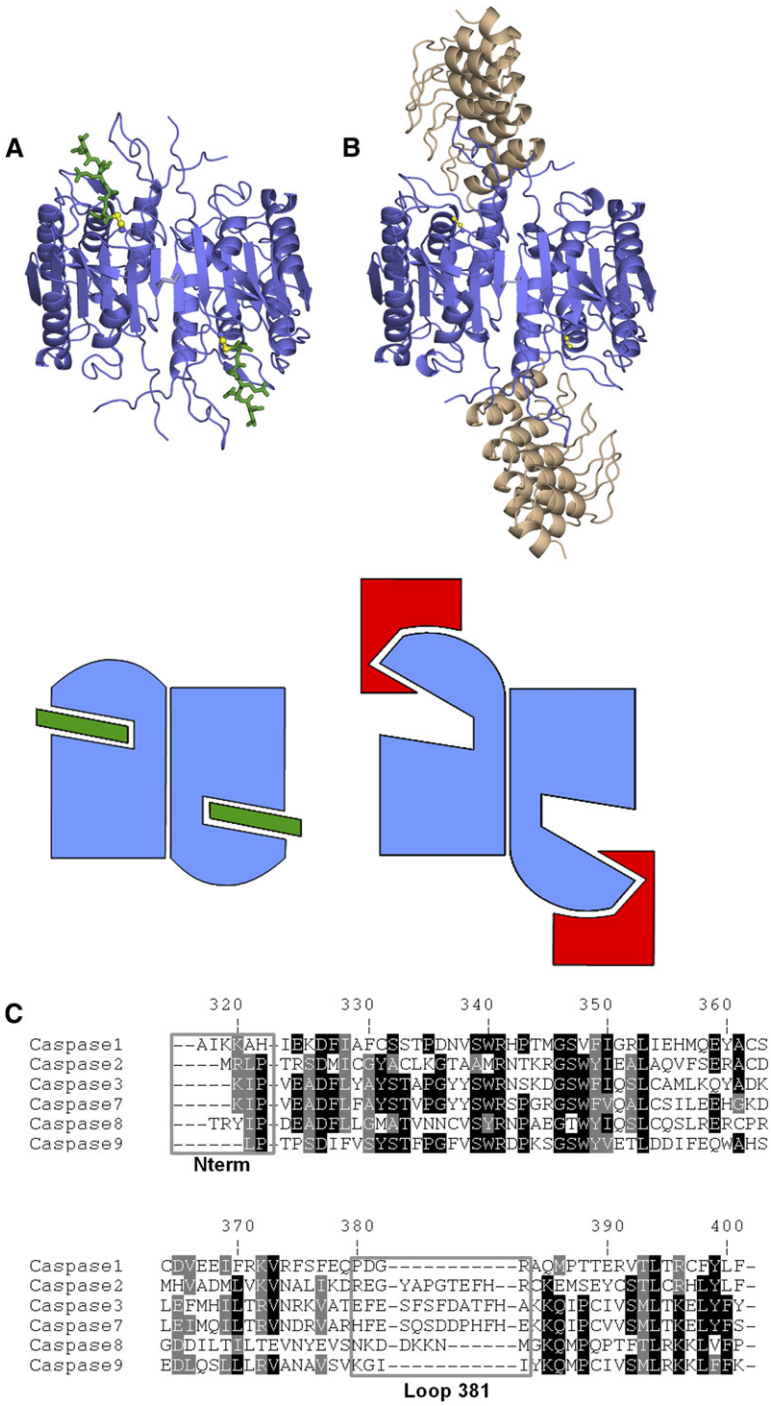

Figure 5. Comparison of Caspase-2 Structures and Sequence Alignment of the β Subunits of Homologous Caspases

(A) Structure and cartoon representation of the caspase-2/LDESD-CHO complex.

(B) Structure and cartoon representation of the caspase-2/AR_F8 complex; the AR_F8 protein binds to loop 381 and the N-terminal part of the symmetry-related β subunit of caspase-2.

(C) Sequence alignment of selected human caspases. The alignment is based on the structures of the individual caspases; the numbering refers to caspase-1. The regions located at the interface of the caspase-2/AR_F8 complex are boxed. Highly conserved residues are shaded in black, and moderately conserved ones are shaded in gray.

active-site cleft, but may include many other epitopes on the surface of the target protein. Some of these epitopes may represent allosteric sites.

An allosteric site in caspase-7 that is located in the central cavity at the dimer interface was reported (Hardy et al., 2004). Here, covalent binding of small-molecule inhibitors at the dimer interface trapped the caspase in an inactive conformation that closely resembles its zymogen form. As shown above, AR_F8 binds primarily to loop 381. This loop forms one side of the active-site cleft. The interaction of Pro275 (381c) and Gly276 (381d) with Phe114 and Tyr122, respectively, of AR_F8 stabilizes a distinct conformation in loop 381; there are structural differences in the S5 and the S4 pockets compared to caspase-2 with a bound substrate analog. The structural restriction of the S5 and S4 pockets by the side chains of Tyr79 and Gln112, respectively, of AR_F8 is most probably responsible for the competitive contribution of inhibition.

Another critical conformational difference compared to the caspase-2/substrate analog structure occurs at the N terminus of the proximal β subunit: the N-terminal loop has a different conformation in the AR_F8-binding structure, and Met209 (319) of caspase-2 interacts with Thr57 of AR_F8 by a hydrophobic contact. This conformation relocates the C-terminal part of the α subunit and displaces the active-site cysteine (Cys285) by 1 Å, misaligning it from its optimal position for nucleophilic attack. Moreover, structural differences are found in loop 341 and the adjacent β strand that forms the bottom of the active-site pocket. In this way, the hydrogen-bond interactions between enzyme and substrate are critically disturbed, which also prevents the proper positioning of substrates and therefore binding of substrate in a mixed-type, inhibitory way.

Allosteric regulation of proteins is highly effective and is known to be a primary means of biological control. Natural and man-made allosteric modulators offer several significant advantages over orthosteric ligands, including greater selectivity and saturability of their effects (Christopoulos, 2002). Allosteric inhibition of DARPins has been reported for both natural ankyrins and DARPins: several crystal structures of the cyclin-dependent kinase 6 (Cdk6) with different natural ankyrin inhibitors of the INK4 family (p16, p18, and p19) illustrate an allosteric inhibition mechanism (Brotherton et al., 1998; Jeffrey et al., 2000; Russo et al., 1998). Recently, the crystal structure of a DARPin, binding and inhibiting aminoglycoside phosphotransferase (3′)-IIIa, a bacterial antibiotic-resistance enzyme, revealed an allosteric inhibition mode as well: the inhibitor bound and stabilized a conformation of the kinase, which can no longer interact with the substrate in a productive fashion (Amstutz et al., 2005; Kohl et al., 2005). While the development of allosteric regulators is difficult and was to date a pure trial-and-error process relying on high-throughput screening (Noble et al., 2004), we believe that our results, together with the previous findings regarding selection of a DARPin kinase inhibitor (Amstutz et al., 2005; Kohl et al., 2005), indicate that (1) DARPins themselves represent an attractive alternative to synthetic inhibitors because they are highly specific due to the fact that they can bind to less-conserved surface regions of a target protein, and that (2) DARPin-target protein complex structures represent an excellent starting point for the generation of novel synthetic inhibitors based on the nonproductive conformation of the enzyme in the complex. Specific caspase inhibitors are indispensable for the validation of pathways, for the discovery of unknown interactions, and for the identification of novel intracellular targets. In contrast to peptide-based caspase-2 inhibitors that inhibit, for instance, the complete VDVADase activity of cell lysates, AR-F8 is able to exclusively inhibit the contribution arising from caspase-2.

While such protein-based inhibitors will currently serve mostly as a discovery tool, future developments in protein uptake and gene therapy may offer broader perspectives for the use of such inhibitory proteins. More immediately, the mechanistic, and especially structural, dissection of their action, as described in this work, may lead to a new approach to small-molecule, cell-permeable inhibitors: by effecting a similar allosteric transition as the inhibitory protein, the problem of individually addressing a member of an enzyme family may be solved, even when the active-site structures of the proteins are almost identical.

EXPERIMENTAL PROCEDURES

Protein Expression and Purification

Two separate expression vectors, derived from pET11d (Novagen), were constructed for the expression of the large p19 ($MetAlaAsn_{150}$–Asp_{316}) and the small p12 ($MetAla_{331}$–Thr_{435}) subunits of human caspase-2 (SwissProt database accession number P42575). An Avi tag sequence (Schatz, 1993) was introduced at the N terminus of p19 to obtain a biotinylated variant of the protein, starting with the sequence MAGLNDIFEAQKIEWHEG. Both the caspase-2 p19 subunit, which was expressed as inclusion bodies, and protein D from phage λ (used as a control) (Yang et al., 2000), expressed as soluble protein, were biotinylated in vivo by using plasmid pBirAcm in *E. coli* BL21 (DE3) (Novagen) and *E. coli* XL-1 Blue (Stratagene), respectively, by following the protocols from Avidity (Denver, CO) and QIAGEN (Hilden, Germany). Efficient biotinylation was confirmed by ELISA, western blot with a streptavidin-alkaline phosphatase conjugate (Roche, Switzerland), and mass spectrometry. The p19 and p12 subunits of both the biotinylated and the untagged variant were expressed as inclusion bodies, and the protease was refolded and purified as described (Schweizer et al., 2003).

DARPins for in vitro inhibition assays were produced in soluble form and purified by using affinity chromatography as described (Kohl et al., 2003). For the production of caspase-3, the genes of the large p17 ($MetSer_{29}$–Asp_{175}) and the small p12 ($MetAlaSer_{175}$–His_{277}) subunits were inserted in the NcoI-BamHI sites of the pET11d plasmids (Novagen). For caspase-8, the genes encoding the large p18 ($MetGlyGlu_{218}$–Asp_{374}) and the small p12 ($MetAlaGlu_{376}$–Asp_{479}) subunits were inserted into the NcoI site of pET11d (Novagen). Expression, refolding, and purification of caspase-3 and caspase-8 were performed as described (Garcia-Calvo et al., 1998, 1999; Thornberry et al., 1997). Caspase-7 and caspase-9 were purchased from Alexis Biochemicals (Lausen, Switzerland).

Ribosome Display with an N3C DARPin Library

The generation of DARPin libraries has been described elsewhere (Binz et al., 2003). Here, an N3C library was used for the selections, encoding DARPins consisting of an N-terminal capping repeat, three internal AR modules containing randomized residues, and a C-terminal capping repeat. The PCR-amplified libraries of the ribosome-display format were transcribed, and three standard ribosome-display selection rounds were performed against immobilized caspase-2 as described (Binz et al., 2004; Hanes and Plückthun, 1997). The RT-PCR product of the genes obtained after the third selection cycle was then used for a single clone analysis.

Combined Solid-Phase Screening for Binders and Inhibitors

The open reading frame of the RT-PCR product encoding the selected DARPins was ligated into pQE30 (QiAgen) via BamHI/HindIII. Single colonies of transformed *E. coli* XL-1 Blue cells (Stratagene) were used for the expression of individual AR proteins. Cells were grown in 1.2 ml Luria Bertani/1% glucose (w/v) medium in 96-well format deep-well plates (Abgene, UK), and proteins were expressed for 3 hr at 37°C after induction with 0.5 mM isopropyl-1-thio-β-D-galactopyranoside. Cell pellets were lysed with 50 μl B-Per II (Pierce) for 10 min at room temperature with shaking, and then the lysates were mixed with 250 μl 50 mM Tris HCl (pH 7.5), 500 mM NaCl. A centrifugation step (5000 rpm, 10 min, 4°C) was applied to pellet cell debris,

Table 1. Statistics for Data Collection and Refinement

Data Collection	
Space group	$P2_1$
Cell dimensions (Å)	a = 58.02, b = 229.21, c = 114.93; α = 90°, β = 90.11°, γ = 90°
Resolution limits (Å)	30–3.24 (3.5–3.24)[a]
Observed reflections	165,291 (34,589)[a]
Unique reflections	92,159 (18,974)[a]
Completeness (%)	98.0 (98.0)[a]
Redundancy	1.79 (1.82)[a]
R_{sym} (% on I)	5.9 (37.9)[a]
I/σ	9.81 (2.41)[a]
Refinement	
Resolution range (Å)	20–3.24
R factor/R_{free} (%)	26.2/30.5
Ordered water molecules	29
Rms deviation from ideal	
Bond lengths (Å)	0.01
Bond angles (°)	1.474
Average B factor (Å^2)	95.82

[a] Numbers in parentheses refer to the highest-resolution shell.

and the supernatants, containing the expressed DARPins, were used for additional experiments.

Caspase-2 was immobilized on Maxisorp 96-well plates (Nunc, Denmark). For the screening for caspase inhibitors, 100 μl each of the crude *E. coli* extracts containing the DARPins was applied to both wells containing immobilized caspase-2 and to wells containing the control (protein D from phage λ). To test for potential inhibitors, a caspase activity assay was performed as described (Stennicke and Salvesen, 1999). Fluorescence of the AMC leaving group was detected at λ_{ex} = 360 nm and λ_{em} = 465 nm after a 20 min incubation at 25°C by using an HTS 7000 Plus Bio Assay Reader (Perkin Elmer). Binding was tested by ELISA with an anti-RGS-His antibody (QIAGEN), an anti-mouse-IgG-alkaline phosphatase conjugate (Pierce), and p-nitrophenylphosphate (Fluka, Switzerland). Protein D from phage λ was used as a negative control for binding specificity for each tested DARPin.

Crystallization and Data Collection

Crystallization

The caspase-2/AR_F8 complex was purified with Superdex 200 HR 10/30 (Amersham Pharmacia, Sweden) size-exclusion chromatography in 50 mM Tris-HOAc (pH 7.5), 50 mM KSCN, 0.5 mM TCEP, concentrated to 20 mg/ml by using an Amicon Ultra-4 (Millipore). Crystallization trials were first performed with the Cartesian MicroSys (Genomic Solutions Ltd., UK) at the nanoliter scale and were subsequently scaled up and optimized. The crystals used for data collection were grown in 1 day at 20°C in a 4 μl hanging drop containing a 1:1 ratio of protein solution:reservoir solution (17% [w/v] PEG 5000-MME, 0.1 M Tris-HOAc [pH 7.2], 0.1 M KSCN, and 30% [v/v] ethylene glycol).

X-Ray Diffraction Data Collection

Diffraction data were collected on a 225 CCD MarResearch detector at the Swiss Light Source PX beamline (Villigen, Switzerland) at a wavelength of 0.899 Å. A single crystal was used for data collection. The crystal diffracted to 3.2 Å resolution. The space group was found to be $P2_1$ (a = 58.02 Å, b = 229.21 Å, c = 114.93 Å, β = 90.11°); there were three enzyme-inhibitor complexes per asymmetric unit. The data (see Table 1) were processed and scaled with XDS (Kabsch, 1988).

Structure Determination and Refinement

The structure was solved by molecular replacement with the program AmoRe (Navaza, 1994), by using the caspase-2/LDESD complex structure (1PYO [Schweizer et al., 2003]) and the DARPin structure E3_5 (1MJ0 [Kohl et al., 2003]) as search models. Using the diffraction data from 10 to 4 Å, AMoRe (Navaza, 1994) indicated the presence in the asymmetric unit of three caspase-2 dimers, each bound to two AR_F8 molecules. The calculated solvent content was 51%. Density modification (CCP4, 1994) (solvent flattening, histogram matching, and 3-fold averaging) yielded phases of sufficient quality to help effective model rebuilding. The program COOT was used for this purpose (Emsley and Cowtan, 2004). After rigid-body refinement with CNS (Brünger et al., 1998) with data from 30 to 3.24 Å, cycles of torsion angle-simulated annealing, conjugate gradient minimization refinement, and B factor refinement were alternated with model rebuilding. NCS restraints were applied throughout the refinement to all protein chains. A bulk solvent correction was also applied. A total of 29 water molecules were introduced in the last phase of the refinement, and the unliganded caspase-2 structure was checked for the presence of equivalent water molecules. The final R value was 26.2%, and the R_{free} was 30.5%.

Enzyme Kinetics

The concentration of the caspase substrate Ac-VDVAD-AMC was determined spectrophotometrically after quantitative hydrolysis by caspase-2 by using an absorption coefficient for the 7-amino-4-methylcoumarin product of 16,000 M^{-1} cm^{-1} at 342 nm (Baici et al., 1996). Initial rates of substrate hydrolysis at 25°C ± 1°C were measured fluorimetrically by using an HTS 7000 Plus Bio Assay Reader (Perkin Elmer) with excitation and emission wavelengths of 360 nm and 465 nm, respectively. The buffer was composed of 100 mM MES (pH 6.50), 10% w/v PEG 600, 10 mM DTT, and 0.1% w/v CHAPS. The Michaelis constant, K_M = 55.3 μM, of Ac-VDVAD-AMC for caspase-2 was determined by fitting the Michaelis-Menten equation to initial velocity data obtained at 15 substrate concentrations. Preliminary measurements suggested that inhibition of caspase-2 by AR_F8 was not of the slow-binding type, and that the interaction was relatively tight. Thus, the inhibition mechanism was investigated in two steps. In the first of these, the inhibition type was diagnosed by using a combination of five substrate concentrations (0.25–4 times K_M) and five inhibitor concentrations in the range of 25–400 nM. Analysis of initial velocity data for the 25 combinations of substrate and inhibitor concentrations were performed with the specific velocity plot, a graphical method suitable for diagnosing linear and hyperbolic inhibition mechanisms (Baici, 1981). This method is based on the general modifier mechanism shown in Scheme 1:

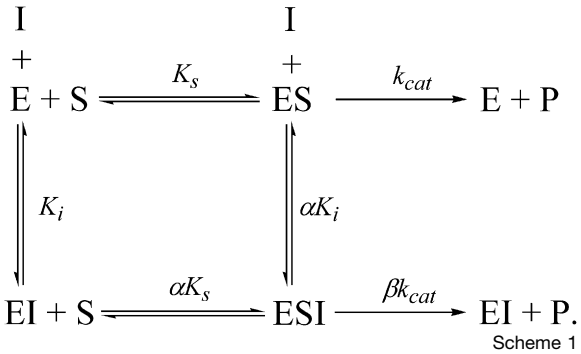

Scheme 1

Here, E represents the free enzyme, S represents the substrate, I represents the AR_F8 inhibitor, and P, collectively, represents the products of the reaction. Other symbols are as follows: K_i = [E][I]/[EI], the competitive inhibitor constant; αK_i = [ES][I]/[ESI], the uncompetitive

inhibitor constant; K_s = [E][S]/[ES], the substrate dissociation constant; αK_s = [EI][S]/[ESI]; k_{cat}, the catalytic rate constant. The dimensionless coefficients α and β characterize the proportion of competitive and uncompetitive character in the inhibition mechanism and the fact that inhibition may be incomplete (hyperbolic inhibition, $\beta < 1$) at saturating inhibitor, respectively. The specific velocity equation is as follows:

$$\frac{v_0}{v_i} = \frac{[I]\left(\frac{1}{\alpha K_i} - \frac{1}{K_i}\right)}{1 + \beta\frac{[I]}{\alpha K_i}} \frac{\sigma}{1+\sigma} + \frac{1 + \frac{[I]}{K_i}}{1 + \beta\frac{[I]}{\alpha K_i}}, \quad (1)$$

where v_0 and v_i are the initial velocities in the absence and in the presence of inhibitor, respectively, and $\sigma = [S]/K_M$; other symbols are as described above. Plots of data derived from Equation 1 (Figure S2), collected at high inhibitor concentrations to avoid inhibitor depletion and thus allowing for the consideration of a value of [I] practically identical to the total inhibitor added, were characteristic of hyperbolic, mixed-type inhibition (Baici, 1981). From the specific velocity plot and its secondary plots, sufficiently precise values of α and β, and a rough estimate of K_i, could be calculated. In a second approach, an accurate value of K_i was obtained by measuring initial velocities at fixed enzyme and substrate concentrations (1 nM and 40 μM, respectively) and several AR_F8 concentrations (Figure 1B). The tight-binding condition and the hyperbolic, mixed-type character of the inhibition were taken into account with the following equation (Szedlacsek et al., 1988):

$$v_i = \frac{v_0}{2}\left[\frac{\alpha+\sigma-\beta(1+\sigma)}{\alpha+\sigma}\right]\left\{\sqrt{\left[\left(\frac{1+\sigma}{\alpha+\sigma}\frac{\alpha K_i}{[E]_t} + \frac{[I]_t}{[E]_t} - 1\right)^2 + 4\frac{1+\sigma}{\alpha+\sigma}\frac{\alpha K_i}{[E]_t}\right]} + \frac{\alpha+\sigma+\beta(1+\sigma)}{\alpha+\sigma-\beta(1+\sigma)} - \frac{1+\sigma}{\alpha+\sigma}\frac{\alpha K_i}{[E]_t} - \frac{[I]_t}{[E]_t}\right\}. \quad (2)$$

In Equation 2, $[I]_t$ is the total inhibitor concentration, and other symbols are the same as described above. Nonlinear regression analysis by using Equation 2 does not allow the simultaneous determination of all parameters from a single titration curve. Therefore, we used the α and β values determined independently with the specific velocity plot, as well as the $\sigma = [S]/K_M$ ratio, as constants, while retaining K_i and the total enzyme concentration $[E]_t$ as parameters to be fitted. Nonlinear regression analysis was performed by using GraphPad Prism version 4.00 for Windows, GraphPad Software, San Diego, CA (www.graphpad.com).

Caspase Activity Assays

Different inhibitors plus AR_F8 were tested in a specificity inhibition test of caspase-2, -3, -7, -8, and -9. The concentrations of all low-molecular mass inhibitor solutions were determined by using an amino acid analyzer (AminoQuant, Hewlett Packard). The caspase-2, -3, -7, and -8 concentrations in the assay were 30 nM, and the peptidic inhibitors or AR_F8 inhibitor was added prior to the measurement at 60 or 150 nM (corresponding to a 2-fold or 5-fold molar excess over enzyme). Caspase-9 was assayed at 150 nM, as its low specific activity did not allow for accurate measurements at 30 nM, and the inhibitors were added at 300 and 750 nM. The following substrates were used (all at 20 μM concentration): Ac-VDVAD-AMC (Calbiochem) for caspase-2 and caspase-3, Ac-DEVD-AMC (Calbiochem) for caspase-7 and caspase-8, and Ac-LEHD-AMC (Alexis Biochemicals) for caspase-9. The initial velocities were determined by following the protocol for the standard caspase activity assay (Stennicke and Salvesen, 1999).

Abbreviations

Ac-, acetyl-; AMC, 7-amino-4-methylcoumarin; -CHO, -aldehyde; CHAPS, 3-[(3-cholamidopropyl)-dimethylammonio]-1-propanesulfonate; DARPin, designed ankyrin repeat protein; DTT, 1,4-dithio-DL-threitol; IAP, inhibitor of apoptosis; LDESD, Leu-Asp-Glu-Ser-Asp; LEHD, Leu-Glu-His-Asp; MES, 2-morpholinoethanesulfonic acid monohydrate; MME, monomethyl ether; PEG, polyethylene glycol; PIDD, p53-induced protein with a death domain; SPR, surface plasmon resonance; TCEP, Tris-(carboxyethyl)-phosphine; VDVAD, Val-Asp-Val-Ala-Asp; VYAD, Val-Tyr-Ala-Asp.

Supplemental Data

Supplemental Data include two figures and are available at http://www.structure.org/cgi/content/full/15/5/625/DC1/.

ACKNOWLEDGMENTS

We thank E. Lenherr and R. Ganesan for providing caspase-8 and caspase-3, P. Mittl and D. Frey are acknowledged for fruitful discussions, and P. Mittl is also acknowledged for critical reading of the manuscript. We gratefully acknowledge the Swiss Light Source, Paul Scherrer Institute, Villigen, Switzerland for providing synchrotron beamtime and excellent support during data collection. This work was supported by the Swiss National Science Foundation grant 3100A-102218 to M.G.G. and by the Baugartenstiftung (Zürich, Switzerland). H.R.V. was supported by CAMP, a specific targeted research project funded by the European Commission. P.A. and H.K.B. are affiliated with the University of Zürich and Molecular Partners AG. A.P. is a shareholder in Molecular Partners AG. Molecular Partners AG is developing designed repeat proteins as binding agents for research, diagnostics, and therapy.

Received: December 21, 2006
Revised: March 9, 2007
Accepted: March 14, 2007
Published: May 15, 2007

REFERENCES

Amstutz, P., Binz, H.K., Parizek, P., Stumpp, M.T., Kohl, A., Grütter, M.G., Forrer, P., and Plückthun, A. (2005). Intracellular kinase inhibitors selected from combinatorial libraries of designed ankyrin repeat proteins. J. Biol. Chem. *280*, 24715–24722.

Baici, A. (1981). The specific velocity plot. A graphical method for determining inhibition parameters for both linear and hyperbolic enzyme inhibitors. Eur. J. Biochem. *119*, 9–14.

Baici, A., Szedlacsek, S.E., Früh, H., and Michel, B.A. (1996). pH-dependent hysteretic behaviour of human myeloblastin (leucocyte proteinase 3). Biochem. J. *317*, 901–905.

Bergeron, L., Perez, G.I., Macdonald, G., Shi, L.F., Sun, Y., Jurisicova, A., Varmuza, S., Latham, K.E., Flaws, J.A., Salter, J.C.M., et al. (1998). Defects in regulation of apoptosis in caspase-2-deficient mice. Genes Dev. *12*, 1304–1314.

Binz, H.K., Stumpp, M.T., Forrer, P., Amstutz, P., and Plückthun, A. (2003). Designing repeat proteins: well-expressed, soluble and stable proteins from combinatorial libraries of consensus ankyrin repeat proteins. J. Mol. Biol. *332*, 489–503.

Binz, H.K., Amstutz, P., Kohl, A., Stumpp, M.T., Briand, C., Forrer, P., Grütter, M.G., and Plückthun, A. (2004). High-affinity binders selected from designed ankyrin repeat protein libraries. Nat. Biotechnol. *22*, 575–582.

Biocca, S., Ruberti, F., Tafani, M., Pierandrei-Amaldi, P., and Cattaneo, A. (1995). Redox state of single chain Fv fragments targeted to the endoplasmic reticulum, cytosol and mitochondria. Biotechnology (N. Y.) *13*, 1110–1115.

Brotherton, D.H., Dhanaraj, V., Wick, S., Brizuela, L., Domaille, P.J., Volyanik, E., Xu, X., Parisini, E., Smith, B.O., Archer, S.J., et al. (1998). Crystal structure of the complex of the cyclin D-dependent kinase Cdk6 bound to the cell-cycle inhibitor p19INK4d. Nature *395*, 244–250.

Brünger, A.T., Adams, P.D., Clore, G.M., DeLano, W.L., Gros, P., Grosse-Kunstleve, R.W., Jiang, J.S., Kuszewski, J., Nilges, M., Pannu, N.S., et al. (1998). Crystallography & NMR system: a new software suite for macromolecular structure determination. Acta Crystallogr. D Biol. Crystallogr. *54*, 905–921.

CCP4 (Collaborative Computational Project, Number 4) (1994). The CCP4 Suite: programs for protein crystallography. Acta Crystallogr. D Biol. Crystallogr. *50*, 760–763.

Ceruti, S., Beltrami, E., Matarrese, P., Mazzola, A., Cattabeni, F., Malorni, W., and Abbracchio, M.P. (2003). A key role for caspase-2 and caspase-3 in the apoptosis induced by 2-chloro-2′-deoxy-adenosine (cladribine) and 2-chloro-adenosine in human astrocytoma cells. Mol. Pharmacol. *63*, 1437–1447.

Christopoulos, A. (2002). Allosteric binding sites on cell-surface receptors: novel targets for drug discovery. Nat. Rev. Drug Discov. *1*, 198–210.

Dirsch, V.M., Kirschke, S.O., Estermeier, M., Steffan, B., and Vollmar, A.M. (2004). Apoptosis signaling triggered by the marine alkaloid ascidemin is routed via caspase-2 and JNK to mitochondria. Oncogene *23*, 1586–1593.

Emsley, P., and Cowtan, K. (2004). Coot: model-building tools for molecular graphics. Acta Crystallogr. D Biol. Crystallogr. *60*, 2126–2132.

Estrov, Z., Thall, P.F., Talpaz, M., Estey, E.H., Kantarjian, H.M., Andreeff, M., Harris, D., Van, Q., Walterscheid, M., and Kornblau, S.M. (1998). Caspase 2 and caspase 3 protein levels as predictors of survival in acute myelogenous leukemia. Blood *92*, 3090–3097.

Ewert, S., Honegger, A., and Plückthun, A. (2004). Stability improvement of antibodies for extracellular and intracellular applications: CDR grafting to stable frameworks and structure-based framework engineering. Methods *34*, 184–199.

Faderl, S., Thall, P.F., Kantarjian, H.M., Talpaz, M., Harris, D., Van, Q., Beran, M., Kornblau, S.M., Pierce, S., and Estrov, Z. (1999). Caspase 2 and caspase 3 as predictors of complete remission and survival in adults with acute lymphoblastic leukemia. Clin. Cancer Res. *5*, 4041–4047.

Fuentes-Prior, P., and Salvesen, G.S. (2004). The protein structures that shape caspase activity, specificity, activation and inhibition. Biochem. J. *384*, 201–232.

Garcia-Calvo, M., Peterson, E.P., Leiting, B., Ruel, R., Nicholson, D.W., and Thornberry, N.A. (1998). Inhibition of human caspases by peptide-based and macromolecular inhibitors. J. Biol. Chem. *273*, 32608–32613.

Garcia-Calvo, M., Peterson, E.P., Rasper, D.M., Vaillancourt, J.P., Zamboni, R., Nicholson, D.W., and Thornberry, N.A. (1999). Purification and catalytic properties of human caspase family members. Cell Death Differ. *6*, 362–369.

Green, I., Christison, R., Voyce, C.J., Bundell, K.R., and Lindsay, M.A. (2003). Protein transduction domains: are they delivering? Trends Pharmacol. Sci. *24*, 213–215.

Guo, Y., Srinivasula, S.M., Druilhe, A., Fernandes-Alnemri, T., and Alnemri, E.S. (2002). Caspase-2 induces apoptosis by releasing pro-apoptotic proteins from mitochondria. J. Biol. Chem. *277*, 13430–13437.

Hanahan, D., and Weinberg, R.A. (2000). The hallmarks of cancer. Cell *100*, 57–70.

Hanes, J., and Plückthun, A. (1997). In vitro selection and evolution of functional proteins by using ribosome display. Proc. Natl. Acad. Sci. USA *94*, 4937–4942.

Hardy, J.A., Lam, J., Nguyen, J.T., O'Brien, T., and Wells, J.A. (2004). Discovery of an allosteric site in the caspases. Proc. Natl. Acad. Sci. USA *101*, 12461–12466.

Jackson, A.L., Bartz, S.R., Schelter, J., Kobayashi, S.V., Burchard, J., Mao, M., Li, B., Cavet, G., and Linsley, P.S. (2003). Expression profiling reveals off-target gene regulation by RNAi. Nat. Biotechnol. *21*, 635–637.

Jeffrey, P.D., Tong, L., and Pavletich, N.P. (2000). Structural basis of inhibition of CDK-cyclin complexes by INK4 inhibitors. Genes Dev. *14*, 3115–3125.

Kabsch, W. (1988). Automatic indexing of rotation diffraction patterns. J. Appl. Crystallogr. *21*, 67–71.

Kohl, A., Binz, H.K., Forrer, P., Stumpp, M.T., Plückthun, A., and Grütter, M.G. (2003). Designed to be stable: crystal structure of a consensus ankyrin repeat protein. Proc. Natl. Acad. Sci. USA *100*, 1700–1705.

Kohl, A., Amstutz, P., Parizek, P., Binz, H.K., Briand, C., Capitani, G., Forrer, P., Plückthun, A., and Grütter, M.G. (2005). Allosteric inhibition of aminoglycoside phosphotransferase by a designed ankyrin repeat protein. Structure *13*, 1131–1141.

Lassus, P., Opitz-Araya, X., and Lazebnik, Y. (2002). Requirement for caspase-2 in stress-induced apoptosis before mitochondrial permeabilization. Science *297*, 1352–1354.

Lo Conte, L., Chothia, C., and Janin, J. (1999). The atomic structure of protein-protein recognition sites. J. Mol. Biol. *285*, 2177–2198.

Navaza, J. (1994). AMoRe: an automated package for molecular replacement. Acta Crystallogr. A *50*, 157–163.

Noble, M.E., Endicott, J.A., and Johnson, L.N. (2004). Protein kinase inhibitors: insights into drug design from structure. Science *303*, 1800–1805.

Robertson, J.D., Enoksson, M., Suomela, M., Zhivotovsky, B., and Orrenius, S. (2002). Caspase-2 acts upstream of mitochondria to promote cytochrome c release during etoposide-induced apoptosis. J. Biol. Chem. *277*, 29803–29809.

Robertson, J.D., Gogvadze, V., Kropotov, A., Vakifahmetoglu, H., Zhivotovsky, B., and Orrenius, S. (2004). Processed caspase-2 can induce mitochondria-mediated apoptosis independently of its enzymatic activity. EMBO Rep. *5*, 643–648.

Russo, A.A., Tong, L., Lee, J.O., Jeffrey, P.D., and Pavletich, N.P. (1998). Structural basis for inhibition of the cyclin-dependent kinase Cdk6 by the tumour suppressor p16INK4a. Nature *395*, 237–243.

Schatz, P.J. (1993). Use of peptide libraries to map the substrate specificity of a peptide-modifying enzyme: a 13 residue consensus peptide specifies biotinylation in *Escherichia coli*. Biotechnology (N. Y.) *11*, 1138–1143.

Schweizer, A., Briand, C., and Grütter, M.G. (2003). Crystal structure of caspase-2, apical initiator of the intrinsic apoptotic pathway. J. Biol. Chem. *278*, 42441–42447.

Scott, C.W., Sobotka-Briner, C., Wilkins, D.E., Jacobs, R.T., Folmer, J.J., Frazee, W.J., Bhat, R.V., Ghanekar, S.V., and Aharony, D. (2003). Novel small molecule inhibitors of caspase-3 block cellular and biochemical features of apoptosis. J. Pharmacol. Exp. Ther. *304*, 433–440.

Sennhauser, G., Amstutz, P., Briand, C., Storchenegger, O., and Grütter, M.G. (2007). Drug export pathway of multidrug exporter AcrB revealed by DARPin inhibitors. PLoS Biol. *5*, e7.

Sevignani, C., Calin, G.A., Cesari, R., Sarti, M., Ishii, H., Yendamuri, S., Vecchione, A., Trapasso, F., and Croce, C.M. (2003). Restoration of fragile histidine triad (FHIT) expression induces apoptosis and suppresses tumorigenicity in breast cancer cell lines. Cancer Res. *63*, 1183–1187.

Siegel, R.M. (2006). Caspases at the crossroads of immune-cell life and death. Nat. Rev. Immunol. *6*, 308–317.

Sledz, C.A., Holko, M., de Veer, M.J., Silverman, R.H., and Williams, B.R.G. (2003). Activation of the interferon system by short-interfering RNAs. Nat. Cell Biol. *5*, 834–839.

Stennicke, H.R., and Salvesen, G.S. (1999). Caspases: preparation and characterization. Methods *17*, 313–319.

Szedlacsek, S.E., Ostafe, V., Serban, M., and Vlad, M.O. (1988). A re-evaluation of the kinetic equations for hyperbolic tight-binding inhibition. Biochem. J. *254*, 311–312.

Talanian, R.V., Quinlan, C., Trautz, S., Hackett, M.C., Mankovich, J.A., Banach, D., Ghayur, T., Brady, K.D., and Wong, W.W. (1997). Substrate specificities of caspase family proteases. J. Biol. Chem. *272*, 9677–9682.

Thornberry, N.A., Rano, T.A., Peterson, E.P., Rasper, D.M., Timkey, T., Garcia-Calvo, M., Houtzager, V.M., Nordstrom, P.A., Roy, S., Vaillancourt, J.P., et al. (1997). A combinatorial approach defines specificities of members of the caspase family and granzyme B. Functional relationships established for key mediators of apoptosis. J. Biol. Chem. *272*, 17907–17911.

Tinel, A., and Tschopp, J. (2004). The PIDDosome, a protein complex implicated in activation of caspase-2 in response to genotoxic stress. Science *304*, 843–846.

Troy, C.M., Rabacchi, S.A., Friedman, W.J., Frappier, T.F., Brown, K., and Shelanski, M.L. (2000). Caspase-2 mediates neuronal cell death induced by beta-amyloid. J. Neurosci. *20*, 1386–1392.

Yang, F., Forrer, P., Dauter, Z., Conway, J.F., Cheng, N., Cerritelli, M.E., Steven, A.C., Plückthun, A., and Wlodawer, A. (2000). Novel fold and capsid-binding properties of the lambda-phage display platform protein gpD. Nat. Struct. Biol. *7*, 230–237.

Accession Numbers

The atomic coordinates have been deposited in the Brookhaven Protein Data Bank with entry code 2P2C.

